Solar Energy Materials & Solar Cells 114 (2013) 71–81

Contents lists available at SciVerse ScienceDirect

Solar Energy Materials & Solar Cells

journal homepage: www.elsevier.com/locate/solmat

Organic photovoltaics with thick active layers (~800 nm) using a high mobility polymer donor

Leanne Murphy [a,b], Wei Hong [a], Hany Aziz [b,c,*], Yuning Li [a,*]

[a] Department of Chemical Engineering, University of Waterloo, 200 University Ave West, Waterloo, Ont. N2L 3G1, Canada
[b] Waterloo Institute for Nanotechnology (WIN), University of Waterloo, 200 University Ave West, Waterloo, Ont. N2L 3G1, Canada
[c] Department of Electrical and Computer Engineering, University of Waterloo, 200 University Ave West, Waterloo, Ont. N2L 3G1, Canada

ARTICLE INFO

Article history:
Received 19 January 2013
Received in revised form
25 February 2013
Accepted 28 February 2013
Available online 27 March 2013

Keywords:
Organic photovoltaics
Inverted configuration
Active layer thickness
Polymer semiconductors
Mobility

ABSTRACT

Rather consistent power conversion efficiencies have been achieved in organic solar cells throughout a wide range of active layer thicknesses (~100 nm to ~800 nm) by using a p-type polymer semiconductor with high hole transport mobility (~1 $cm^2 V^{-1} s^{-1}$) as the donor, and $PC_{61}BM$ as the acceptor. A comparison between standard and inverted device configurations demonstrates that the inverted configuration is more suitable for achieving thicker active layers when a high hole mobility donor is used. We attribute this to the longer hole collection path in the inverted structure, which can benefit from using a high hole mobility material. Our results will be very useful for the development of new semiconductor materials and the design of device structures for more feasible manufacturing of large area OPV devices via high speed roll-to-roll printing processes.

1. Introduction

Organic photovoltaics (OPVs) are widely acknowledged as a promising technology to convert sunlight into electricity inexpensively [1–3]. Currently, relatively low power conversion efficiency (PCE) is still a major barrier that precludes large-scale commercialization of this technology. Steady improvements in PCE have been made over the last decade, mainly due to the design of new materials and optimization of device processing [4,5]. Increasing the active layer thickness is customarily envisioned as a method to improve device efficiency through greater light absorption and thus, increased exciton generation. For the majority of high efficiency OPVs, however, the optimal thickness for best performance is around 100 nm [6–12]. A slight change to the optimal active layer thickness normally causes a dramatic drop in the photovoltaic performance. From a manufacturing perspective, very thin active layers and a narrow window of tolerable thickness (i.e. a few tens of nm) present formidable challenges in high throughput roll-to-roll processing [13,14].

One of the greatest obstacles in achieving thick active layers is the inability of electrons and holes to traverse the increased distance due to charge recombination that originates from low charge carrier mobilities of the donor and acceptor materials. High charge carrier mobility (~10^{-3} $cm^2 V^{-1} s^{-1}$ or greater) is therefore necessary to prevent charge losses if the active layer thickness reaches several hundred nanometers [15]. Thicker active layers, combined with the fact that holes and electrons often have very different mobilities, lead to space charge limited photocurrents that usually hamper the cell performance [16–18]. This unbalanced charge transport of holes versus electrons decreases the fill factor (*FF*) by promoting charge recombination [19,20]. In the case of bulk heterojunction (BHJ) solar cells utilizing high mobility donors, the charge transport balance is often achieved by increasing the concentration of the acceptor material (i.e. a fullerene derivative), thereby increasing the apparent electron mobility [21]. Having balanced mobilities is highly important in the case of low band gap polymers, which tend to be more susceptible to space charge formation due to their higher charge carrier densities [22].

A correlation between OPV efficiency and hole mobility of the donor has previously been suggested [23]. Poly(3-hexylthiophene) (P3HT), a commonly used donor polymer, is generally considered to be a high mobility polymer with reported field-effect mobility up to 0.1 $cm^2 V^{-1} s^{-1}$ in organic thin film transistors (OTFTs) [24]. Relatively high PCE has previously been achieved in OPV devices with active layers just over 300 nm using a blend of P3HT and [6,6]-phenyl C61-butyric acid methyl ester ($PC_{61}BM$) [25,26]. More recently, it was demonstrated that P3HT:PCBM OPV devices could maintain consistent PCEs at active layer thicknesses up to and beyond 800 nm [27,28].

Polymers containing diketopyrrolopyrrole (DPP) as an electron acceptor building block are currently of great interest as donor

* Corresponding authors at: Waterloo Institute for Nanotechnology (WIN), University of Waterloo, 200 University Ave West, Waterloo, Ont. N2L 3G1, Canada. Tel.: +1 519 888 4567; fax: +1 519 888 4347.
E-mail addresses: hany.aziz@ecemail.uwaterloo.ca (H. Aziz), yuning.li@uwaterloo.ca (Y. Li).

0927-0248/$ - see front matter © 2013 Elsevier B.V. All rights reserved.
http://dx.doi.org/10.1016/j.solmat.2013.02.033

materials for OPVs [29]. In addition to having low band gaps for optimal power conversion of sunlight [30–33], many DPP-containing polymers are attractive for their high hole mobility [34,35]. Recently our group developed a p-type polymer semiconductor with a DPP core, PDQT (Fig. 1), which showed high hole transport mobility ($\sim$1 $cm^2\ V^{-1}\ s^{-1}$) in OTFTs [36], almost a tenfold increase over that of P3HT.

PDQT is a rather attractive donor material for OPVs due to its low band gap ($\sim$1.2 eV) [36], and its energy levels, which are highly compatible with those of $PC_{61}BM$, a commonly used fullerene acceptor material (see Supporting information). The high mobility of PDQT is expected to lead to higher *FF* values, even in thicker active layers, due to reduced recombination. Recently, Liu et al. reported OPV devices prepared with PDQT. An efficiency of 5.6% was achieved using an active layer thickness of $\sim$140 nm with $PC_{71}BM$ as the acceptor [37], demonstrating the high potential of this donor material for the OPV application. In this study, we carried out systematic investigations on OPVs with various donor/acceptor (D/A) ratios and active layer thicknesses in both standard and inverted configurations. The results show that using PDQT as the donor allows efficiency to be maintained over a wide thickness range ($\sim$100 nm to $\sim$800 nm). This is attributed to the high hole mobility of the donor material, PDQT. The results suggest that this material is potentially suitable for the manufacture of large area OPV devices through a high throughput roll-to-roll printing process.

2. Experimental details

2.1. Materials

PDQT was synthesized according to the literature [36]. The number average molecular weight (M_n) and the polydispersity index (PDI) are 21,100 and 2.72, respectively, measured by using a high-temperature gel-permeation chromatography (HT-GPC) at 140 °C using 1,2,4-trichlorobenzene as eluent and polystyrene as standards. PEDOT:PSS (P VP AI 4083) was purchased from Clevios. $PC_{61}BM$ was purchased from 1-Material Inc. All other materials were purchased from Sigma-Aldrich and used without further purification.

2.2. Standard OPV device fabrication

Glass substrates coated with indium tin oxide (ITO, $\sim$15 Ω/square), purchased from Luminescence Technology Corporation, were cleaned by sonicating in acetone, soap solution (1% Micro 90 in water) and isopropyl alcohol then dried at 100 °C overnight. A 40–45 nm layer of PEDOT:PSS was spin-coated (3000 rpm, 60 s) onto the ITO substrates followed by annealing at $\sim$165 °C for 10 min in air. The active layer was deposited in a glove box by spin-coating a solution of PDQT:$PC_{61}BM$ in chloroform/o-dichlorobenzene (4:1 v/v) containing 0.5% diiodooctane (DIO) at a certain speed for 60 s. Different thicknesses were obtained by varying the spin-coating speed. The samples were dried at 60 °C for 10 min on a hot plate. A layer of LiF ($\sim$1 nm), followed by a layer of aluminum ($\sim$100 nm), were deposited by thermal evaporation through a shadow mask under a pressure of $\sim 10^{-5}$ mbar. The areas of the devices on each substrate were 0.1 cm^2, 0.125 cm^2 and 0.175 cm^2.

2.3. Inverted OPV device fabrication

A 30 nm layer of ZnO was deposited onto cleaned ITO substrates by spin-coating a zinc acetate solution (33 mg/mL) in ethanol and ethanolamine (0.9% v/v) at 700 rpm for 60 s, followed by annealing at $\sim$180 °C for 60 min in air. The active layer was then deposited similarly to the procedure described for the standard devices. A layer of MoO_3 ($\sim$6 nm) and a layer of silver ($\sim$100 nm) were sequentially deposited by thermal evaporation through a shadow mask under a pressure of $\sim 10^{-5}$ mbar.

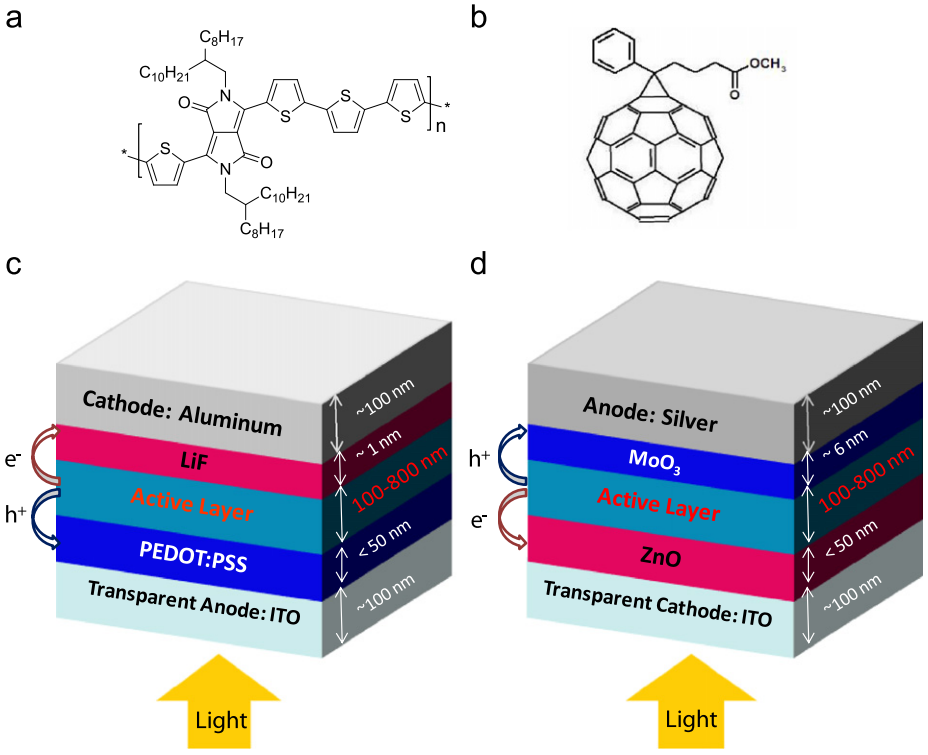

Fig. 1. The chemical structures: (a) PDQT and (b) $PC_{61}BM$, and OPV configurations: (c) standard and (d) inverted.

2.4. Hole-only device fabrication

A 40–45 nm layer of PEDOT:PSS was spin-coated (3000 rpm, 60 s) onto cleaned ITO substrates followed by annealing at ~165 °C for 10 min in air. The active layer was then deposited similarly as above. A layer of MoO_3 (~6 nm), followed by a layer of silver (~100 nm), were deposited by thermal evaporation through a shadow mask under a pressure of $\sim 10^{-5}$ mbar.

2.5. Electron-only device fabrication

A 30 nm layer of ZnO was deposited onto cleaned ITO substrates by spin-coating a zinc acetate solution (33 mg/mL) in ethanol and ethanolamine (0.9% v/v) at 700 rpm for 60 s, followed by annealing at ~180 °C for 60 min in air. The active layer was then deposited similarly as above. A layer of LiF (~1 nm), followed by a layer of aluminum (~100 nm), were deposited by thermal evaporation through a shadow mask under a pressure of $\sim 10^{-5}$ mbar.

2.6. Instrumentation

UV–vis absorption measurements were performed using a Thermo Scientific GENESYS™ 20 Spectrophotometer. Film thicknesses were measured using a Veeco Dektak 8 profiler at a tip force of 1–3 mg. Atomic Force Microscopy (AFM) imaging was carried out on a Dimension 3100 Scanning Probe Microscope. Current–voltage (J–V) analysis was conducted under simulated AM 1.5G irradiation (100 mW/cm^2) using an ABET Technologies Sun 2000 Solar Simulator. Shunt resistance (R_{shunt}) and series resistance (R_{series}) were extracted from the illuminated J–V characteristics using the two-diode analytical model [38].

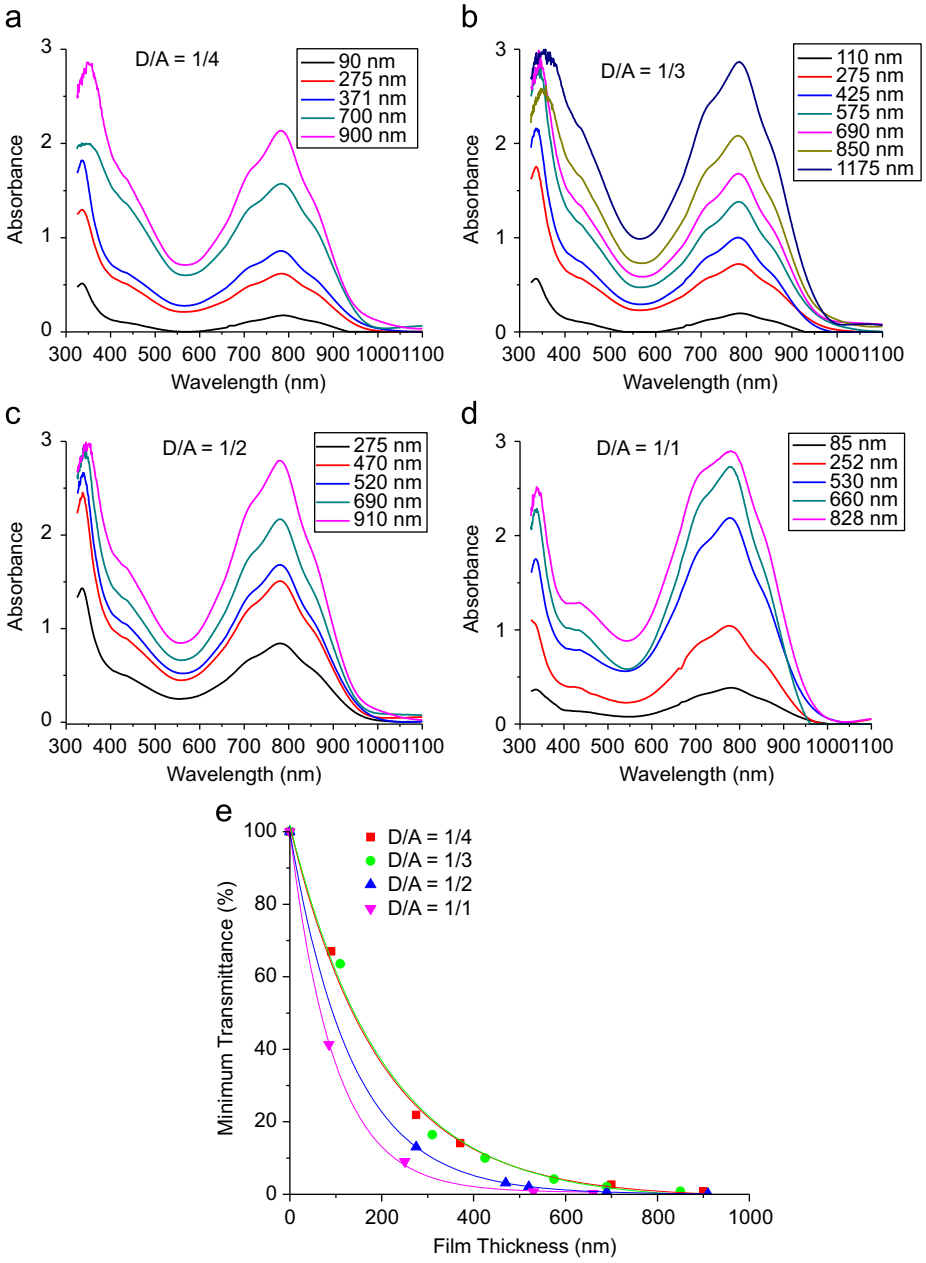

Fig. 2. UV–vis spectroscopic graphs and transmittance plots of PDQT:$PC_{61}BM$ blend films prepared at various active layer thicknesses and D/A ratios. Transmittance values were determined from the Beer–Lambert equation using the maximum absorbance values at 780 nm.

3. Results and discussion

Two types of OPV configuration were adopted in this study: standard and inverted (Fig. 1). The main difference between the two configurations is the electrode positioning with respect to the light source: in the standard configuration, the transparent electrode, indium tin oxide (ITO), acts as the hole-collecting anode, whereas in the inverted configuration, ITO acts as the electron-collecting cathode. OPV devices with various D/A ratios (PDQT/$PC_{61}BM$=1/4, 1/3, 1/2 and 1/1, by weight) were fabricated in order to study the effect of altering electron and hole collection capacities on OPV characteristics.

In theory, J_{sc} increases with increasing charge generation or photon absorption, and thus thicker active layers would be beneficial. To study the absorption characteristics of the active layer, PDQT:$PC_{61}BM$ films of various D/A ratios and thicknesses were prepared and analyzed by UV–vis absorption measurements (Fig. 2 and Supporting information). The pure PDQT film absorbs strongly in the region ranging from 600 nm to 950 nm [36], while $PC_{61}BM$ contributes mainly in the short wavelength region below 400 nm [39]. The lowest absorption of the blend films appears at ~500 nm. Transmittance at 780 nm, where the maximum absorption of PDQT is located, was calculated using the Beer–Lambert equation and is plotted against active layer thickness (Fig. 2e). As expected, transmittance decreases exponentially with increasing active layer thickness. Therefore we expect that for an OPV comprising this material blend, the vast majority of exciton generation (~90%) will occur within the first 250 nm of the active layer for the highest D/A ratio of 1/1, and 450 nm for the lowest D/A ratio of 1/4. Considering that the transmittance values were taken at the maximum absorption, the PDQT:$PC_{61}BM$ active layer thickness is required to be greater than ~250–450 nm, depending on the D/A ratio, in order to harvest the majority of sunlight.

The PDQT:$PC_{61}BM$ blends with varied thickness were first tested in OPVs having a standard configuration. A layer of PEDOT:PSS was spin-coated onto the surface of the ITO anode to act as a hole extraction layer (HEL). A commonly used LiF electron extraction layer (EEL) was added between the active layer and the aluminum cathode to effectively extract electrons and block holes. Fig. 3 shows the PCE and related parameters (*FF*, J_{sc}, and

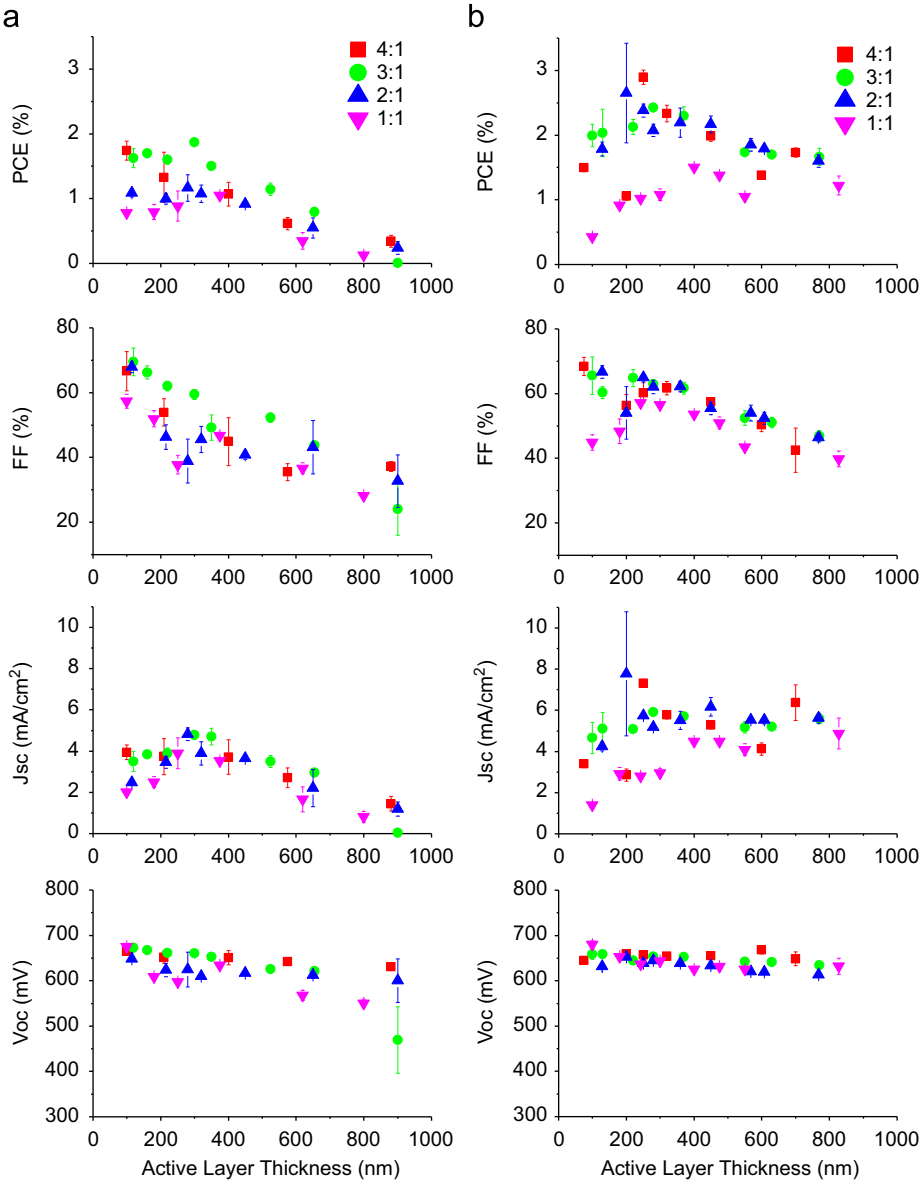

Fig. 3. Power conversion efficiency (PCE), open circuit voltage (V_{oc}), fill factor (*FF*) and short-circuit current density (J_{sc}) of OPV devices at various active layer thicknesses with (a) standard and (b) inverted configurations using various D/A ratios. See Supporting information for selected *J*–*V* curves.

V_{oc}) for these devices. The PCE for the D/A=1/1 devices reached a maximum value of 1.1% at a thickness of 375 nm, but was considerably lower (only 0.1%) for the devices with the thickest active layer (~800 nm). Devices with D/A ratios of 1/2 and 1/3 showed similar trends to the devices with D/A=1/1. In general, the PCE for all of the D/A=1/3 devices was considerably higher than other D/A ratios, with the maximum PCE of 1.9% achieved at a thickness of 300 nm. In contrast to other ratios, the PCE of the D/A=1/4 devices was highest at the lowest thickness of ~100 nm, but also dropped as the thickness was increased. Thus it appears that increasing the active layer thickness beyond 300 nm in standard devices leads to a decrease in PCE for all D/A ratios. We can better understand this trend by looking at the effects of the active layer thickness, as well as the shunt and series resistances, on each of the efficiency parameters.

Shunt resistance (R_{shunt}) is indicative of the charge losses due to recombination and trapping [40]. To prevent leakage currents, a sufficiently high R_{shunt} is required [41]. Series resistance (R_{series}), on the other hand, is a result of ohmic losses arising from obstructed charge flow. The presence of charge traps in the bulk, energy barriers at the interfaces, and the formation of space charges due to poor charge collection versus generation rates may lead to a large R_{series} [40]. A large R_{series} would generally cause a decrease in *FF*, but also results in lower J_{sc} if its value exceeds 10–100 Ω cm^2 [42].

In all D/A ratios, the maximum *FF* was observed for the device with the thinnest active layer (~100 nm) in each series. As the active layer thickness increases, *FF* decreases monotonically. The steady decrease in *FF* from the lowest to the highest thickness is reflected in the changes of R_{shunt} and R_{series} (Fig. 4). R_{shunt} in the standard devices was found to decrease with increasing thickness in all ratios up to ~400 nm; it then becomes fairly constant. This suggests that recombination increases with increasing active layer thickness and reaches its maximum at a thickness of ~400 nm. Variations can be observed amongst the different D/A ratios. In comparison with the 1/1 and 1/2 ratios, the 1/3 ratio demonstrates higher R_{shunt} at each thickness, suggesting that this D/A ratio offers a better charge balance. The higher content of $PC_{61}BM$ in the 1/3 ratio blends provides a greater pathway through which the electrons can flow, thereby reducing recombination. However, a further increase in the $PC_{61}BM$ content (D/A=1/4) causes R_{shunt} to drop to the same level as the devices with D/A=1/2 or 1/1, probably due to the discontinuity of the donor phase, which hampers hole transport.

R_{series} for each D/A ratio is relatively constant until the thickness reaches ~400 nm. At thicknesses greater than 400 nm, a marked increase in R_{series} is observed. This demonstrates an increase in ohmic losses due to increasing thickness, and suggests that space charge, which leads to bimolecular recombination, is prevalent at greater active layer thicknesses. Variations in R_{series} amongst the different D/A ratios are present, with the 1/3 ratio displaying the lowest R_{series} at each thickness. This is again probably due to a better charge balance attained with the improved pathway (the $PC_{61}BM$ phase) for electron transport.

As predicted from the absorbance data, J_{sc} for all D/A ratios is found to increase with increasing active layer thickness up to ~350–400 nm (Fig. 3), due to improved light harvesting. Beyond this thickness, J_{sc} decreases gradually to very low values. For the D/A=1/1 blends, for example, J_{sc} at 800 nm is only ~1 mA cm^{-2}, about 25% of the maximum value of 4 mA cm^{-2} obtained at ~250 nm. This decrease in J_{sc} for devices with thicknesses greater than ~350–400 nm can be attributed to the notable increase in R_{series} (Fig. 4), and thus reduced charge collection.

The highest V_{oc} of ~640–670 mV was achieved at the lowest thickness of ~100 nm for all D/A ratios. However, V_{oc} decreases very slowly with increasing active layer thickness. The influence

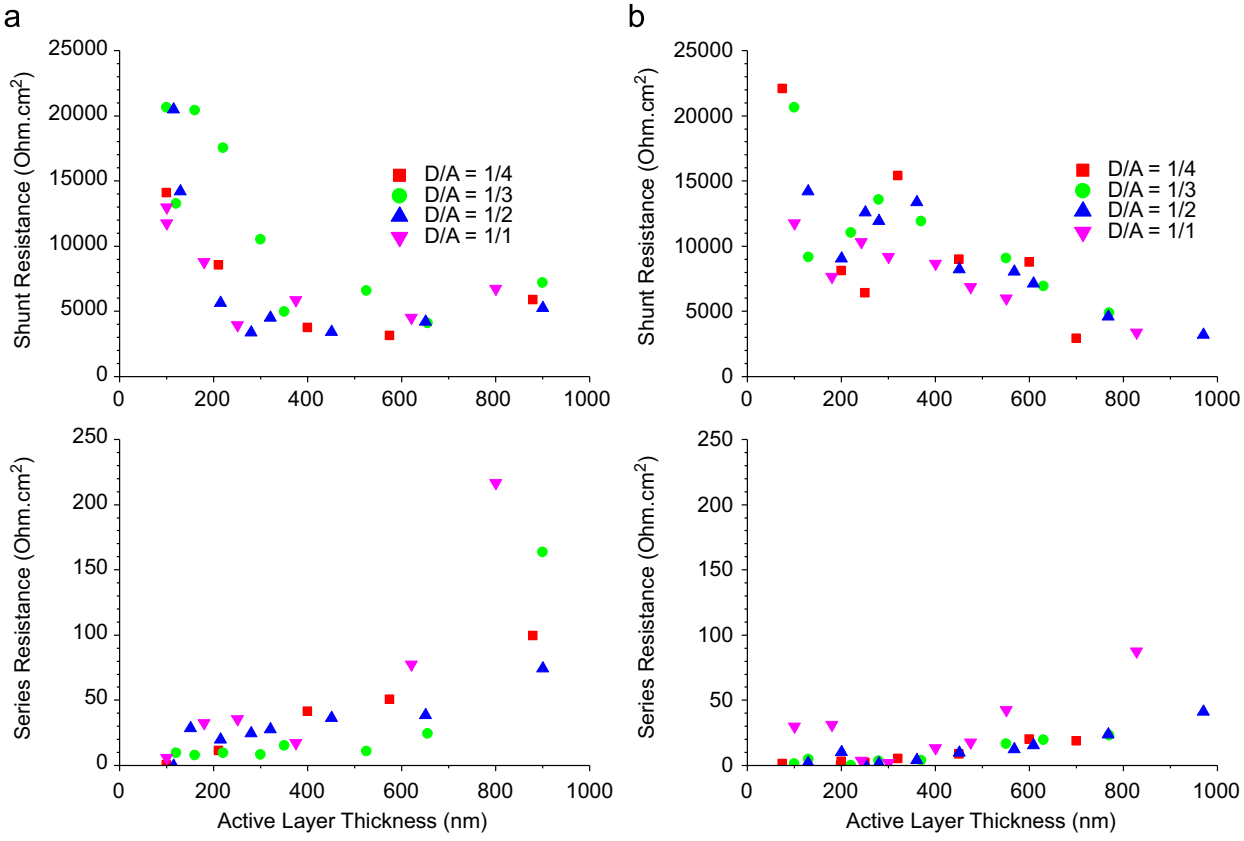

Fig. 4. Shunt resistance and series resistance of OPV devices at various active layer thicknesses with (a) standard and (b) inverted configurations using various D/A ratios.

of the D/A ratio on V_{oc} seems subtle: the lower ratios (1/4 and 1/3) appear to have only slightly higher V_{oc} values than the higher ratios (1/2 and 1/1). Based on the above results, it seems that to achieve consistently good photovoltaic performance in standard OPV devices, the thickness of the PDQT:$PC_{61}BM$ active layer needs to be kept between 100 nm and 400 nm. The optimal thickness is determined by the balance achieved between light harvesting and recombination.

Recently, the inverted architecture has gained increasing popularity due to its higher stability in air [43–45]. Inverted OPV devices have also been found to afford high efficiencies at high active layer thicknesses [26,46]. We therefore also tested PDQT in the inverted OPV device configuration (Fig. 1), in which transparent ITO was used as the bottom cathode and silver was used as the top anode. A thin layer (~30 nm) of ZnO, prepared by spin-coating a precursor solution followed by thermal annealing (180 °C), was inserted between the ITO and the active layer for collecting electrons as well as blocking holes. A thin layer (~6 nm) of MoO_3 was deposited on top of the active layer and beneath the silver anode, for collecting holes and blocking electrons.

Fig. 3 shows the PCE and related parameters (*FF*, J_{sc}, and V_{oc}) for these inverted devices. The *FF* of devices with D/A=1/1 increases with increasing active layer thickness and reaches its maximum value of ~55% at ~250 nm. Further increasing the active layer thickness causes a gradual decrease in *FF*. For devices with lower D/A ratios (1/2, 1/3, and 1/4), the *FF* decreases steadily as the active layer thickness increases from ~100 nm to ~800 nm. However, the *FF* values of the inverted devices are generally much higher than those of the standard devices. In sharp contrast, the decline in R_{shunt} occurs much more gradually in the inverted devices. R_{shunt} values of inverted devices remain above ~5000 Ω cm^2 until the thickness reaches ~700 nm (Fig. 4). This suggests that recombination is suppressed more effectively in the inverted devices than in the standard devices.

For the inverted devices with D/A ratios of 1/2, 1/3, and 1/4, R_{series} values remain at a low level of $<10\ \Omega\ cm^2$ until the thickness reaches ~400 nm. At thicknesses greater than 400 nm, R_{series} values increase, but at a much slower pace compared with the standard devices. Devices with a D/A ratio of 1/1 showed higher R_{series} values than did devices with lower D/A ratios. For inverted devices with various D/A ratios, the trend of R_{series} versus thickness agrees with the trend of *FF*.

The difference between standard and inverted device performance is most remarkable when comparing their J_{sc} values (Fig. 3). In the active layer thickness range of ~100–300 nm, the J_{sc} of inverted devices increases when the thickness increases from ~100 nm to ~300 nm, a similar trend to the one observed for the standard devices. However, the J_{sc} values remain almost constant up to a thickness of ~800 nm, which is strikingly different from the standard devices, in which the J_{sc} decreases significantly at thicknesses beyond ~300 nm. These observations again demonstrate the reduction in recombination within the inverted device architecture at higher active layer thicknesses.

At lower thicknesses of ~100 nm, the V_{oc} values of inverted devices are similar to those of standard devices. However, the V_{oc} of inverted devices remains almost at a constant value of ~650 mV throughout the various thicknesses (~100–800 nm) and various D/A ratios, probably due to less ohmic losses (lower R_{series} values).

In general, the inverted OPV devices showed much higher efficiencies than the standard devices (Fig. 3). For inverted devices with D/A ratios of 1/4, 1/3, and 1/2, the maximum average PCEs of 2.3%–2.8% were achieved at active layer thicknesses of ~200–300 nm. While the PCE for the 1/4 ratio devices drops sharply when the active layer thickness deviates from 300 nm, the PCE for devices with D/A=1/3 or 1/2 remains quite consistent at 1.5%–2.5% throughout the thickness range tested (~100 nm to ~800 nm). Although devices with a D/A ratio of 1/1 displayed lower efficiencies (~1%–1.5%), their performance also shows little dependence on thickness, consistent with devices having other D/A ratios.

We attribute the markedly different photovoltaic performances of standard versus inverted devices to the much higher hole mobility of the donor material versus the electron mobility of the acceptor material used in this study, which makes the inverted architecture more favorable from a charge collection standpoint. The proposed mechanism is illustrated in Fig. 5, which is in agreement with arguments presented in the literature [47–49]. Since illumination occurs through the bottom ITO electrode in both cell architectures, the majority (~90%) of excitons are generated within the first ~250–450 nm of the active layer adjacent to the ITO, as predicted by the UV–vis data. The photogenerated holes and electrons will travel toward the anode and cathode, where they are respectively collected. In a standard device, the electrons travel towards the top cathode through the $PC_{61}BM$ domains, whereas the holes move towards the bottom ITO anode through the PDQT domains. Since charges are created closer to the ITO electrode, the majority of electrons have to travel a longer distance to reach the electron-collecting LiF/Al cathode, whereas the hole collection distance to the PEDOT:PSS/ITO anode is much shorter. Combined with the fact that the electron mobility of $PC_{61}BM$ is much lower than the hole mobility of PDQT, the standard device configuration inherently leads to much poorer electron collection capacity in comparison to that of holes. As the active layer thickness increases, the electron collection distance increases, which further aggravates the situation. As such, increasing the active layer thickness leads to charge accumulation and recombination in the active layer, resulting in a decrease in both *FF* and J_{sc}. On the other hand, in inverted devices, the conduction paths for electrons and holes are reversed, with holes now traveling a longer distance. As a result, the *FF* and J_{sc} of inverted devices remain relatively unchanged over a wide thickness range since the hole mobility of the PDQT donor is much higher.

In order to verify that hole conduction in the PDQT:$PC_{61}BM$ blends is much higher than electron conduction, we utilized hole-only and electron-only devices (Fig. 6a and b, respectively) that were designed and fabricated following previously published methodology [50–56]. For hole-only devices, a structure consisting of ITO/PEDOT:PSS/PDQT:$PC_{61}BM$/MoO_3/Ag was used, while for electron-only devices, a structure of ITO/ZnO/PDQT:$PC_{61}BM$/LiF/Al was adopted. We measured the current density–voltage (*J*–*V*) characteristics in the dark to study changes in hole and electron conduction in these devices, respectively, as the thickness varies. A D/A ratio of 1/3 was chosen due to the high performance of both standard and inverted devices at this ratio. For these measurements, a positive bias, defined as the ITO being at a more positive potential relative to the metal electrode, was used. Under such as a bias, holes flow across the PDQT:$PC_{61}BM$ layer and are collected by the MoO_3/Ag electrode in the hole-only devices, whereas electrons flow across the PDQT:$PC_{61}BM$ layer and are collected by the ZnO/ITO electrode in the electron-only devices. Therefore the flow direction of holes or electrons from the active layer to the contact in these test devices is the same as in the inverted OPV devices. Fig. 6a and b shows the *J*–*V* characteristics obtained from a series of these devices with various PDQT:$PC_{61}BM$ layer thicknesses. As expected, increasing the thickness leads to an increase in overall resistance of all devices, reflected in the lower *J* for any given *V*. However, the changes are much greater in the case of the electron-only devices. For example, in the hole-only devices, increasing the thickness of the active layer by a factor of five (i.e. from 108 nm to 550 nm) generally leads to a decrease in current by approximately one order of magnitude, whereas a similar increase in thickness

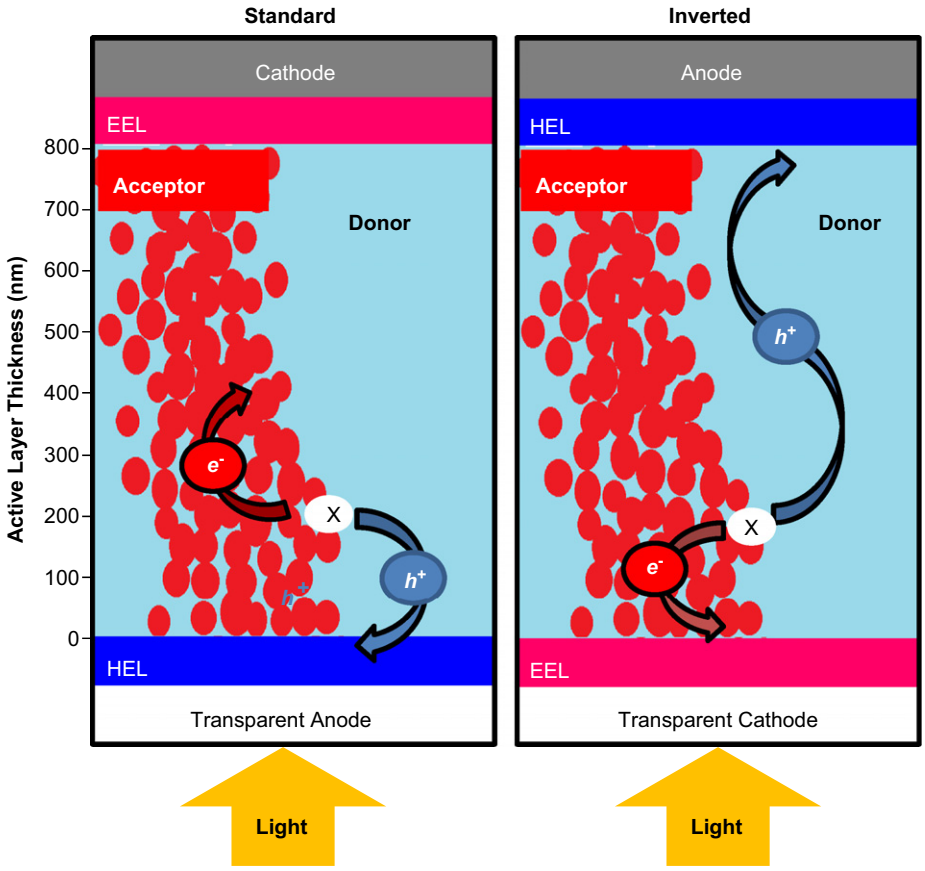

Fig. 5. A schematic description of hole and electron transport in standard and inverted OPV devices. The majority of excitons (x) are created in the first ~250–400 nm of the active layer closest to the light source. In the standard device configuration, the thickness is limited by the distance that the electrons (e^-) are able to move. In the inverted device configuration the thickness is limited by the distance that the holes (h^+) are able to move. A donor with high hole mobility therefore is favoured for the inverted structure.

(i.e. from 120 nm to 630 nm) in the electron-only devices, leads to a decrease in current by more than two orders of magnitude. This clearly shows that hole transport is much easier in the PDQT:$PC_{61}BM$ blend layers, verifying our previous argument that the good performance of the D/A blend layers in inverted devices is due to the higher hole transport.

Hole and electron mobilities are often calculated from the J–V characteristics of such devices using the space charge limited current (SCLC) method [51,53–56]. Analysis of a log J–log V plot reveals a quadratic region that corresponds to the accumulation of space charge and is therefore considered trap-free. In this region, charge mobility is measured according to the Mott–Gurney equation [51,56,57]. The hole and electron mobility values for the hole-only and electron-only devices with varied active layer thicknesses at a D/A ratio of 1/3 were calculated and plotted in Fig. 6c (also see Supporting information). The hole and electron mobilities are comparable at a low active layer thickness: 1.2×10^{-3} $cm^2\,V^{-1}\,s^{-1}$ for the hole-only devices with an active layer thickness of 140 nm and 1.35×10^{-3} $cm^2\,V^{-1}\,s^{-1}$ for the electron-only devices with an active layer thickness of 120 nm. The electron mobility falls in the range of 0.6–5.3 $\times10^{-3}$ $cm^2\,V^{-1}\,s^{-1}$ in the thickness range of 120–630 nm. However, the hole mobility is strongly dependent on the active layer thickness. As the thickness increases from 140 nm to 550 nm, the hole mobility increases dramatically from 1.2×10^{-3} to 2.0×10^{-2} $cm^2\,V^{-1}\,s^{-1}$. Apparently, hole transport is much more efficient than electron transport in the PDQT:$PC_{61}BM$ blend layers, particularly as the active layer gets thicker.

Alstrup et al. [27] also implemented the inverted OPV configuration to demonstrate that the PCE of P3HT:PCBM devices is maintained with increasing active layer thickness (up to 800 nm). All efficiency parameters increased significantly below 150 nm, the region in which carrier generation and transport occur. In thicknesses beyond 300 nm, where mainly hole transport occurs, current continued to increase due to increasing absorption, whereas V_{oc} remained steady and FF decreased at approximately the same rate as the increase in current. Zeng et al. [28], on the other hand, reported that the PCE of standard OPV devices having as-cast P3HT:PCBM active layers decreases as the thickness increases beyond 130 nm. Interestingly, after the devices were thermally annealed, the highest PCE was obtained at a high thickness of 830 nm. It was also observed that the PCE was quite consistent (2.3%–3.1%) over a wide range of thicknesses, from 370 nm to 1200 nm. This was explained by thermally induced vertical phase separation of the donor and acceptor phases, in which PCBM is concentrated next to the top surface, facilitating electron transport. In addition, thermal diffusion of Li^+ ions to the active layer was believed to be beneficial in thick layers through the formation of Li^+PCBM^- complexes.

In principle, the different photovoltaic performances between standard and inverted devices may also arise from vertical phase separation effects, which can lead to different charge collection capacities in the two device configurations [58–61]. For example, it has been suggested that in some cases the concentration of $PC_{61}BM$ is higher in the lower part of the active layer. If this is the case, in our inverted devices, the higher concentration of the acceptor at the bottom of the active layer would facilitate the electron transport towards the bottom cathode (ZnO/ITO), resulting in improved performance of inverted cells. The vertical gradient

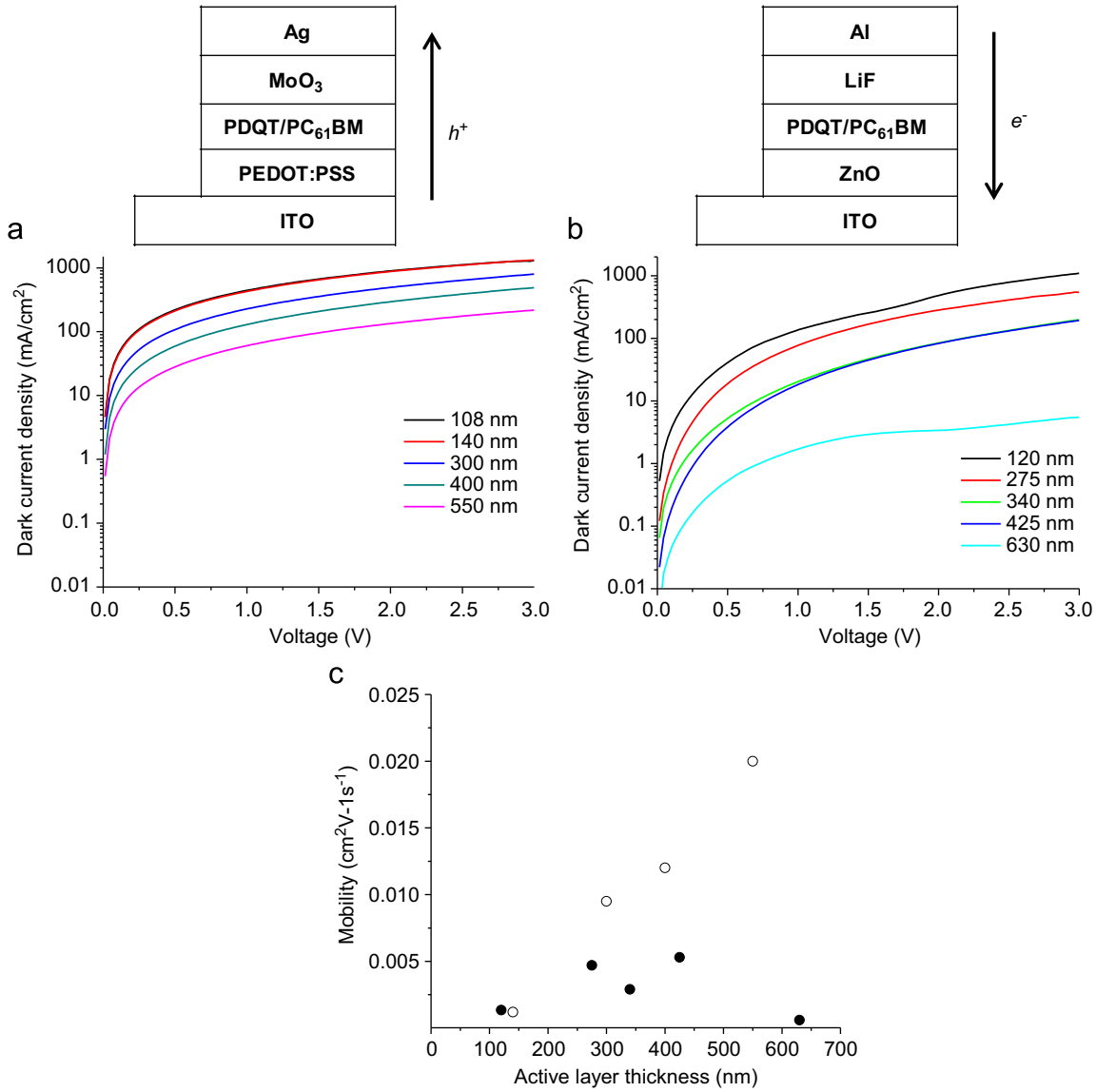

Fig. 6. Dark current densities of the PDQT:$PC_{61}BM$ blends (D/A=1/3) in (a) hole-only and (b) electron-only devices at various active layer thicknesses (Device area=0.125 cm^2). (c) Calculated mobilities of hole-only (open circles) and electron-only (filled circles) devices at various active layer thicknesses.

distribution of PDQT and $PC_{61}BM$ would be influenced by properties of the substrate surface and the active layer thickness. Variations in the gradient distribution would result in changes to the surface morphology of the active layer on different substrate surfaces and at varied active layer thicknesses. In our standard devices, the active layer was spin-coated onto the PEDOT:PSS layer on the ITO-coated glass, whereas in the inverted devices, the active layer was spin-coated onto the ZnO-covered ITO-coated glass. The atomic force microscopic (AFM) images of the active layer films with a D/A ratio of 1/3 on these two types of substrate surfaces are shown in Fig. 7. There are almost no differences in morphology among the films with similar thicknesses. The images obtained for the films on the same substrate with three drastically different thicknesses also showed very similar surface morphologies, suggesting that there is no obvious vertical gradient distribution of PDQT and $PC_{61}BM$ in either device configuration. These results therefore suggest that the dramatically different photovoltaic performances observed for standard and inverted devices are unlikely caused by the vertical or lateral phase separation of their active layers.

It has previously been suggested that the inverted configuration holds the promise of thicker active layers when produced with donor materials that have high hole mobility [47–49]. In standard devices, no material reported in the literature other than P3HT has been able to maintain high PCE beyond the 100–200 nm range. With inverted devices, Peet et al. found that high PCE could be maintained up to a thickness of 400 nm using a polymer (4,4′-bis(alkyl)dithieno[3,2-b:2′,3′-d]silole) and (2,5-bis(thiophen-2-yl)thiazole[5,4–d]thiazole copolymer) with relatively high mobility (10^{-2} cm^2 V^{-1} s^{-1} [46]) in combination with $PC_{61}BM$, which has similar electron mobility (2.4×10^{-2} cm^2 V^{-1} s^{-1} [62]). Here we show that the use of a higher mobility donor material, such as PDQT, allows the PCE of inverted devices to be maintained over a much wider active layer thickness range. In our case, a PCE that is 70% of its peak value was achieved at a thickness as high as 770 nm. In contrast, the PCE of standard OPVs at this thickness is only ~20% of its peak value. Active layers with a thickness as high as ~800 nm and a very wide tolerable thickness range (~100–800 nm) are well suited for conventional printing techniques, such as screening printing, that can be used for low cost, high

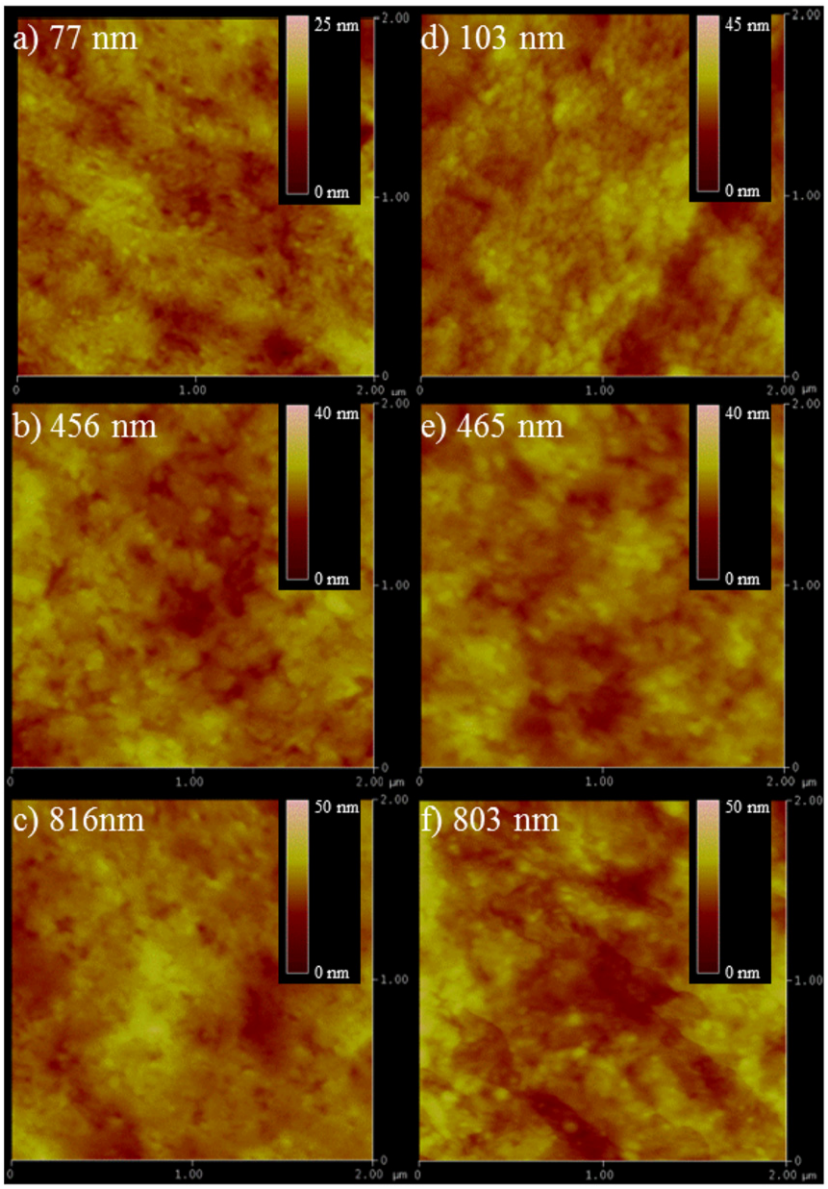

Fig. 7. AFM images (2 μm × 2 μm) of PDQT:$PC_{61}BM$ (1/3) films spin coated on ITO/PEDOT:PSS (a, b, and c) and ITO/ZnO substrates (d, e, and f) at different active layer thicknesses.

throughput processing [14]. Furthermore, D/A ratios of 1/4, 1/3 and 1/2 gave very similar performance even though the charge carrier mobility of PDQT is almost 40 times greater than that of $PC_{61}BM$. This suggests that PCE is not very sensitive to the D/A ratio when a high mobility donor material is used in an inverted configuration, thus providing even wider latitude for easier and much more feasible large scale production of OPVs.

4. Conclusions

We have found that using a high hole mobility polymer, PDQT, allows the fabrication of OPVs with thicker active layers (~100 nm to ~800 nm) without undermining the photovoltaic parameters, especially in the inverted configuration. A comparison between standard and inverted devices demonstrates that the inverted configuration is more suitable for achieving thicker active layers when using a high hole mobility donor. We attribute this to the high hole mobility of the donor phase that helps achieve a longer hole collection path in the inverted configuration.

Additionally, the results of this study demonstrate that the thickness dependence of PCE is governed by the charge collection distance of the carrier going towards the electrode farther from the light source. For inverted devices the mobility of the donor is more critical, whereas balancing the hole and electron mobilities is less important. This suggests that the mobility of the acceptor may be more relevant in standard devices and that acceptors with high electron mobility ($\sim 1\ cm^2\ V^{-1}\ s^{-1}$) may lead to similarly thick active layers in the standard device configuration. Our results show that high mobility of the donor and/or acceptor materials, as well as a suitable device configuration, are key factors for achieving high performance OPV devices with thick active layers.

Acknowledgments

The authors thank the Natural Sciences and Engineering Research Council (NSERC) of Canada for providing the Discovery Grants and Engage Grants and Jon Hollinger and Prof. Dwight Seferos of

University of Toronto for the HT-GPC measurements of PDQT. LM thanks WIN of University of Waterloo for providing the WIN Nanoscholarship. The authors thank Graeme Williams and Uyxing Vongsaysy for valuable technical discussants.

Appendix A. Supporting information

Supplementary information associated with this article can be found in the online version at http://dx.doi.org/10.1016/j.solmat.2013.02.033.

References

[1] C.J. Brabec, Organic photovoltaics: technology and market, Solar Energy Materials and Solar Cells 83 (2004) 273–292.
[2] T.D. Nielsen, C. Cruickshank, S. Foged, J. Thorsen, F.C. Krebs, Business, market and intellectual property analysis of polymer solar cells, Solar Energy Materials and Solar Cells 94 (2010) 1553–1571.
[3] N. Espinosa, R. García-Valverde, A. Urbina, F.C. Krebs, A life cycle analysis of polymer solar cell modules prepared using roll-to-roll methods under ambient conditions, Solar Energy Materials and Solar Cells 95 (2011) 1293–1302.
[4] J. Nelson, Polymer:fullerene bulk heterojunction solar cells, Materials Today 14 (2011) 462–470.
[5] J. Peet, M.L. Senatore, A.J. Heeger, G.C. Bazan, The role of processing in the fabrication and optimization of plastic solar cells, Advanced Materials 21 (2009) 1521–1527.
[6] Y. Liang, Z. Xu, J. Xia, S.T. Tsai, Y. Wu, G. Li, C. Ray, L. Yu., For the bright future-bulk heterojunction polymer solar cells with power conversion efficiency of 7.4%, Advanced Materials 22 (2010) E135–138.
[7] Y. Liang, D. Feng, Y. Wu, S.-T. Tsai, G. Li, C. Ray, L. Yu, Highly efficient solar cell polymers developed via fine-tuning of structural and electronic properties, Journal of the American Chemical Society 131 (2009) 7792–7799.
[8] S.H. Park, A. Roy, S. Beaupré, S. Cho, N. Coates, J.S. Moon, D. Moses, M. Leclerc, K. Lee, A.J. Heeger, Bulk heterojunction solar cells with internal quantum efficiency approaching 100%, Nature Photonics 3 (2009) 297–303.
[9] G. Ren, E. Ahmed, S.A. Jenekhe, Non-fullerene acceptor-based bulk heterojunction polymer solar cells: engineering the nanomorphology via processing additives, Advanced Energy Materials 1 (2011) 946–953.
[10] P. Sonar, G.-M. Ng, T.T. Lin, A. Dodabalapur, Z.-K. Chen, Solution processable low bandgap diketopyrrolopyrrole (DPP) based derivatives: novel acceptors for organic solar cells, Journal of Materials Chemistry 20 (2010) 3626–3636.
[11] G.D. Sharma, P. Suresh, J.A. Mikroyannidis, M.M. Stylianakis, Efficient bulk heterojunction devices based on phenylenevinylene small molecule and perylene–pyrene bisimide, Journal of Materials Chemistry 20 (2010) 561–567.
[12] C.H. Woo, T.W. Holcombe, D.A. Unruh, A. Sellinger, J.M.J. Fréchet, Phenyl vs alkyl polythiophene: a solar cell comparison using a vinazene derivative as acceptor, Chemistry of Materials 22 (2010) 1673–1679.
[13] Y. Sun, C.J. Takacs, S.R. Cowan, J.H. Seo, X. Gong, A. Roy, A.J. Heeger, Efficient, air-stable bulk heterojunction polymer solar cells using MoO(x) as the anode interfacial layer, Advanced Materials 23 (2011) 2226–2230.
[14] C.J. Brabec, J.R. Durrant, Solution-processed organic solar cells, MRS Bulletin 33 (2008) 670–675.
[15] M.C. Scharber, D. Mühlbacher, M. Koppe, P. Denk, C. Waldauf, A.J. Heeger, C.J. Brabec, Design rules for donors in bulk-heterojunction solar cells — towards 10% energy-conversion efficiency, Advanced Materials 18 (2006) 789–794.
[16] V.D. Mihailetchi, H. Xie, B. de Boer, L.M. Popescu, J.C. Hummelen, P.W.M. Blom, L.J.A. Koster, Origin of the enhanced performance in poly (3-hexylthiophene): [6,6]-phenyl C61-butyric acid methyl ester solar cells upon slow drying of the active layer, Applied Physics Letters 89 (2006) 012107-1–012107-3.
[17] V.D. Mihailetchi, J. Wildeman, P.W.M. Blom, Space-charge limited photocurrent, Physical Review Letters 94 (2005) 1–4.
[18] L.J.A. Koster, V.D. Mihailetchi, H. Xie, P.W.M. Blom, Origin of the light intensity dependence of the short-circuit current of polymer/fullerene solar cells, Applied Physics Letters 87 (2005) 203502-1–203502-3.
[19] L.J.A. Koster, V.D. Mihailetchi, P.W.M. Blom, Ultimate efficiency of polymer/fullerene bulk heterojunction solar cells, Applied Physics Letters 88 (2006) 093511-1–093511-3.
[20] P. Peumans, S.R. Forrest, Separation of geminate charge-pairs at donor–acceptor interfaces in disordered solids, Chemical Physics Letters 398 (2004) 27–31.
[21] E. von Hauff, J. Parisi, V. Dyakonov, Field effect measurements on charge carrier mobilities in various polymer-fullerene blend compositions, Thin Solid Films 511–512 (2006) 506–511.
[22] J.D. Kotlarski, D.J.D. Moet, P.W.M. Blom, Role of balanced charge carrier transport in low band gap polymer: fullerene bulk heterojunction solar cells, Journal of Polymer Science Part B: Polymer Physics 49 (2011) 708–711.
[23] J. Chen, Y. Cao, Development of novel conjugated donor heterojunction photovoltaic devices, Accounts of Chemical Research 42 (2009) 1709–1718.
[24] H. Sirringhaus, N. Tessler, R.H. Friend, Integrated optoelectronic devices based on conjugated polymers, Science 280 (1998) 1741–1744.
[25] A.J. Moulé, J.B. Bonekamp, K. Meerholz, The effect of active layer thickness and composition on the performance of bulk-heterojunction solar cells, Journal of Applied Physics 100 (2006) 094503-1–094503-7.
[26] M.S. White, D.C. Olson, S.E. Shaheen, N. Kopidakis, D.S. Ginley, Inverted bulk-heterojunction organic photovoltaic device using a solution-derived ZnO underlayer, Applied Physics Letters 89 (2006) 143517-1–143517-3.
[27] J. Alstrup, M. Jørgensen, A.J. Medford, F.C. Krebs, Ultra fast and parsimonious materials screening for polymer solar cells using differentially pumped slot-die coating, ACS Applied Materials and Interfaces 2 (2010) 2819–2827.
[28] L. Zeng, C.W. Tang, S.H. Chen, Effects of active layer thickness and thermal annealing on polythiophene:fullerene bulk heterojunction photovoltaic devices, Applied Physics Letters 97 (2010) 053305-1–053305-3.
[29] S. Qu, H. Tian, Diketopyrrolopyrrole (DPP)-based materials for organic photovoltaics, Chemical Communications 48 (2012) 3039–3051.
[30] G.-Y. Chen, C.-M. Chiang, D. Kekuda, S.-C. Lan, C.-W. Chu, K.-H. Wei, Synthesis and characterization of a narrow-bandgap polymer containing alternating cyclopentadithiophene and diketo-pyrrolo-pyrrole units for solar cell applications, Journal of Polymer Science Part A: Polymer Chemistry 48 (2010) 1669–1675.
[31] L. Huo, J. Hou, H.-Y. Chen, S. Zhang, Y. Jiang, T.L. Chen, Y. Yang, Bandgap and molecular level control of the low-bandgap polymers based on 3,6-dithiophen-2-yl-2,5-dihydropyrrolo[3,4-c] pyrrole-1,4-dione toward highly efficient polymer solar cells, Macromolecules 42 (2009) 6564–6571.
[32] J. Jo, D. Gendron, A. Najari, J.S. Moon, S. Cho, M. Leclerc, A.J. Heeger, Bulk heterojunction solar cells based on a low-bandgap carbazole-diketopyrrolopyrrole copolymer, Applied Physics Letters 97 (2010) 203303-1–203303-3.
[33] W.-H. Lee, S.K. Son, K. Kim, S.K. Lee, W.S. Shin, S.-J. Moon, I.N. Kang, Synthesis and characterization of new selenophene-based donor-acceptor low-bandgap polymers for organic photovoltaic cells, Macromolecules 45 (2012) 1303–1312.
[34] H. Chen, Y. Guo, G. Yu, Y. Zhao, J. Zhang, D. Gao, H. Liu, Y. Liu, Highly π-extended copolymers with diketopyrrolopyrrole moieties for high-performance field-effect transistors, Advanced Materials 24 (2012) 4618–4622.
[35] J.S. Lee, S.K. Son, S. Song, H. Kim, D.R. Lee, K. Kim, M.J. Ko, D.H. Choi, B. Kim, J.H. Cho, Importance of solubilizing group and backbone planarity in low band gap polymers for high performance ambipolar field-effect transistors, Chemistry of Materials 24 (2012) 1316–1323.
[36] Y. Li, P. Sonar, S.P. Singh, M.S. Soh, M. van Meurs, J. Tan, Annealing-free high-mobility diketopyrrolopyrrole-quaterthiophene copolymer for solution-processed organic thin film transistors, Journal of the American Chemical Society 133 (2011) 2198–2204.
[37] F. Liu, Y. Gu, C. Wang, W. Zhao, D. Chen, A.L. Briseno, T.P. Russell, Efficient polymer solar cells based on a low bandgap semi-crystalline DPP polymer-PCBM blends, Advanced Materials 24 (2012) 3947–3951.
[38] B. Amrouche, A. Guessoum, M. Belhamel, A simple behavioural model for solar module electric characteristics based on the first order system step response for MPPT study and comparison, Applied Energy 91 (2012) 395–404.
[39] J.-H. Huang, C.-P. Lee, Z.-Y. Ho, D. Kekuda, C.-W. Chu, K.-C. Ho, Enhanced spectral response in polymer bulk heterojunction solar cells by using active materials with complementary spectra, Solar Energy Materials and Solar Cells 94 (2010) 22–28.
[40] A. Moliton, J.-M. Nunzi, How to model the behaviour of organic photovoltaic cells, Polymer International 55 (2006) 583–600.
[41] H. Hoppe, N.S. Sariciftci, Organic solar cells: an overview, Journal of Materials Research 19 (2004) 1924–1945.
[42] J.D. Servaites, S. Yeganeh, T.J. Marks, M.A. Ratner, Efficiency enhancement in organic photovoltaic cells: consequences of optimizing series resistance, Advanced Functional Materials 20 (2010) 97–104.
[43] Y. Şahin, S. Alem, R. de Bettignies, J.-M. Nunzi, Development of air stable polymer solar cells using an inverted gold on top anode structure, Thin Solid Films 476 (2005) 340–343.
[44] S.K. Hau, H.-L. Yip, N.S. Baek, J. Zou, K. O'Malley, A.K.-Y. Jen, Air-stable inverted flexible polymer solar cells using zinc oxide nanoparticles as an electron selective layer, Applied Physics Letters 92 (2008) 253301-1–253301-3.
[45] F. Zhang, X. Xu, W. Tang, J. Zhang, Z. Zhuo, J. Wang, J. Wang, Z. Xu, Y. Wang, Recent development of the inverted configuration organic solar cells, Solar Energy Materials and Solar Cells 95 (2011) 1785–1799.
[46] J. Peet, L. Wen, P. Byrne, S. Rodman, K. Forberich, Y. Shao, N. Drolet, R. Gaudiana, G. Dennler, D. Waller, Bulk heterojunction solar cells with thick active layers and high fill factors enabled by a bithiophene-co-thiazolothiazole push–pull copolymer, Applied Physics Letters 98 (2011) 043301-1–043301-3.
[47] J.D. Kotlarski, P.W.M. Blom, Impact of unbalanced charge transport on the efficiency of normal and inverted solar cells, Applied Physics Letters 100 (2012) 013306-1–013306-3.
[48] C. Waldauf, M. Morana, P. Denk, P. Schilinsky, K. Coakley, S.A. Choulis, C.J. Brabec, Highly efficient inverted organic photovoltaics using solution based titanium oxide as electron selective contact, Applied Physics Letters 89 (2006) 233517-1–233517-3.

[49] T.J.K. Brenner, I. Hwang, N.C. Greenham, C.R. McNeill, Device physics of inverted all-polymer solar cells, Journal of Applied Physics 107 (2010) 114501-1–114501-9.
[50] V.D. Mihailetchi, H. Xie, B. de Boer, L.J.A. Koster, P.W.M. Blom, Charge transport and photocurrent generation in poly(3-hexylthiophene):methanofullerene bulk-heterojunction solar cells, Advanced Functional Materials 16 (2006) 699–708.
[51] J.H. Park, J.S. Kim, J.H. Lee, W.H. Lee, K. Cho, Effect of annealing solvent solubility on the performance of poly(3-hexylthiophene)/methanofullerene solar cells, Journal of Physical Chemistry C 113 (2009) 17579–17584.
[52] G. Williams, Q. Wang, H. Aziz, The photo-stability of polymer solar cells: contact photo-degradation and the benefits of interfacial layers, Advanced Functional Materials, http://dx.doi.org/10.1002/adfm.201202567, in press.
[53] G. Ren, P.-T. Wu, S.A. Jenekhe, Enhanced performance of bulk heterojunction solar cells using block copoly(3-alkylthiophene)s, Chemistry of Materials 22 (2010) 2020–2026.
[54] Z.B. Wang, M.G. Helander, M.T. Greiner, J. Qiu, Z.H. Lu, Carrier mobility of organic semiconductors based on current–voltage characteristics, Journal of Applied Physics 107 (2010) 034506-1–034506-4.
[55] C. Goh, R.J. Kline, M.D. McGehee, E.N. Kadnikova, J.M.J. Fréchet, Molecular-weight-dependent mobilities in regioregular poly(3-hexyl-thiophene) diodes, Applied Physics Letters 86 (2005) 122110-1–122110-3.
[56] V. Shrotriya, Y. Yao, G. Li, Y. Yang, Effect of self-organization in polymer/fullerene bulk heterojunctions on solar cell performance, Applied Physics Letters 89 (2006) 063505-1–063505-3.
[57] P.N. Murgatroyd, Theory of space-charge-limited current enhanced by Frenkel effect, Journal of Physics D: Applied Physics 3 (1970) 151–156.
[58] M. Campoy-Quiles, T. Ferenczi, T. Agostinelli, P.G. Etchegoin, Y. Kim, T.D. Anthopoulos, P.N. Stavrinou, D.D.C. Bradley, J. Nelson, Morphology evolution via self-organization and lateral and vertical diffusion in polymer: fullerene solar cell blends, Nature Materials 7 (2008) 158–164.
[59] Z. Xu, L.-M. Chen, G. Yang, C.-H. Huang, J. Hou, Y. Wu, G. Li, C.-S. Hsu, Y. Yang, Vertical phase separation in poly(3-hexylthiophene):fullerene derivative blends and its advantage for inverted structure solar cells, Advanced Functional Materials 19 (2009) 1227–1234.
[60] J.-S. Kim, P.K.H. Ho, C.E. Murphy, R.H. Friend, Phase separation in polyfluorene-based conjugated polymer blends: lateral and vertical analysis of blend spin-cast thin films, Macromolecules 37 (2004) 2861–2871.
[61] A.C. Arias, N. Corcoran, M. Banach, R.H. Friend, J.D. MacKenzie, W.T.S. Huck, Vertically segregated polymer-blend photovoltaic thin-film structures through surface-mediated solution processing, Applied Physics Letters 80 (2002) 1695–1697.
[62] J. Nakamura, K. Murata, K. Takahashi, Relation between carrier mobility and cell performance in bulk heterojunction solar cells consisting of soluble polythiophene and fullerene derivatives, Applied Physics Letters 87 (2005) 132105-1–132105-3.